6th World Congresses of Structural and Multidisciplinary Optimization
Rio de Janeiro, 30 May - 03 June 2005, Brazil

Topology optimization using the finite volume method

A. Gersborg-Hansen[1,2], M. P. Bendsøe[1] and O. Sigmund[2]

[1]Department of Mathematics, Technical University of Denmark, DK-2800 Lyngby, Denmark
Correspondence to M.P.Bendsoe@mat.dtu.dk

[2]Department of Mechanical Engineering, Technical University of Denmark, DK-2800 Lyngby, Denmark

1. Abstract
This papers addresses the use of the finite volume method (FVM) for topology optimization of a heat conduction problem. Issues pertaining to the sensitivity analysis and the application of the FVM to non-homogeneous material distribuions are considered in some detail and example test problems are used to illustrate the effect of applying the FVM as an analysis tool for design optimization.

2. Keywords: Topology optimization, heat conduction, finite volume method, sensitivity analysis.

3. Introduction
In flow problems such as incompressible viscous flows the finite element method (FEM) has in the fluid mechanics community found little application for subsonic flows. Although the FEM is derived from the fundamental principle of virtual work, the discrete implementation of the incompressibility constraint causes problems. Furthermore the conservation of mass on each element can not be guaranteed. Moreover, some element choices give spurious oscillations in the physical pressure field. These issues are serious drawbacks, which motivates the use of other methods, such as the finite volume method (FVM).

Topology optimization for Stokes flow problems for the design of energy efficient fluid devices has recently been investigated in [1], and the effect of inertia in the the non–linear case has been treated in [2], [3] and [4]. These papers share the use of the finite element method (FEM) for solving the underlying physical problem, following the tradition in the structural optimization community.

In transport problems, a possible new area of application for topology optimization, the FVM is a relevant numerical scheme (see [5]) since it guarantees elementwise conservation of the variables, as described in [6] – a property not shared by the FEM. Conservation of mass is very critical in reactive flows since it is related to the well–posedness of the mathematical model.

Motivated by the existence of advanced finite volume solvers used in the fluid mechanic community ([7, 8]), the present paper considers the solution of a topology optimization problem using the finite volume method (FVM) for solving the underlying physical problem. The prototype problem under consideration is a heat diffusion problem, cf., [9] (see also [10], [11], [12], and [13] for advanced examples involving heat conduction).

4. FVM for heat conduction
A simple physical problem of steady state heat diffusion is used to demonstrate the basic technicalities of solving a topology optimization problem involving the use of the FVM. We follow the textbook [14] in setting up the FVM equations.

Let $\Omega \subset \mathbb{R}^2$ be a spatial design domain with boundary $\Gamma = \overline{\Gamma_D \cup \Gamma_N}, \Gamma_D \cap \Gamma_N = \emptyset$ partitioned in a Dirichlet (D) and a Neumann (N) part. On Ω we consider the steady state heat equation given in its strong form and with homogeneous boundary conditions

$$-\nabla \cdot (k\mathbf{I}\nabla T) + f = 0 \quad \text{in} \quad \Omega \tag{1a}$$

$$T = 0 \quad \text{on} \quad \Gamma_D \tag{1b}$$

$$(k\mathbf{I}\nabla T) \cdot \mathbf{n} = 0 \quad \text{on} \quad \Gamma_N \tag{1c}$$

where T is the temperature, $k\mathbf{I}$ the isotropic diffusion tensor, f the volumetric heat source and $\mathbf{n}$ an outward unit normal vector. Moreover, the heat flux is defined as $\mathbf{q} = k\mathbf{I}\nabla T$. The physical meaning is that the temperature at Γ_D is fixed at $T = 0$ and the boundary Γ_N is insulated.

With topology optimization in mind we consider a state field (temperature) and a design field (conductivity) on Ω. The discrete representation of the two fields is seen in Fig. 1 and is based on nodal values of the fields, in

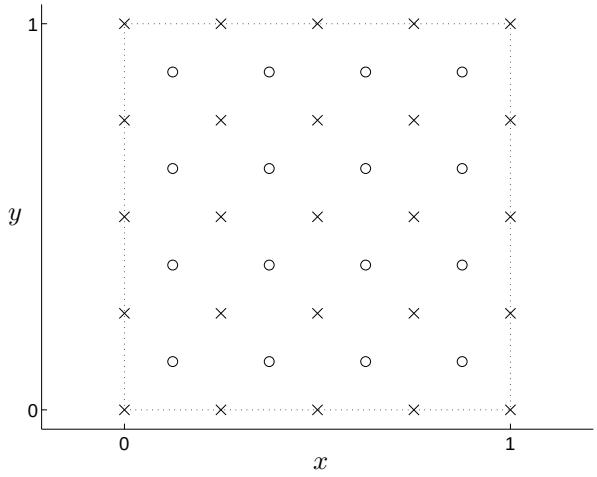

Figure 1: Spatial domain with state nodes '$\times$', design nodes '$\circ$', and physical boundary '$\cdots$'.

two regular grids, one for each field. In the following section a topology optimization problem is formulated such that an optimal conduction field $k = k(\mathbf{x})$ is determined using topology optimization [9].

The FVM form of the heat equation is obtained by integrating over subdomains Ω_e and applying the Gauss theorem:

$$\int_{\Omega_e} (-\nabla \cdot (k\mathbf{I}\nabla T) + f) = 0 \quad \Rightarrow \quad \int_{\partial\Omega_e} -(k\mathbf{I}\nabla T) \cdot \mathbf{n} = \int_{\Omega_e} -f \quad \forall e \tag{2}$$

where $\mathbf{n}$ is a unit normal vector.

For the dicretization at hand (cf., Fig. 1) the FVM test volumes Ω_e are obtained by defining a surrounding volume for each node in the domain, see Fig. 2. On each state volume we require the governing FVM equation (2) to be satisfied using a finite difference approximation for the temperature gradient. In order to calculate the heat flux at the element interface, some average value of the conductivity is used. Two averages have been tested

$$\langle k \rangle_{\mathcal{I}} = \begin{cases} \dfrac{1}{n} \displaystyle\sum_{i=1}^{n} k_i & \text{(arithmetic)} \\ n \left(\displaystyle\sum_{i=1}^{n} \frac{1}{k_i} \right)^{-1} & \text{(harmonic)} \end{cases} \tag{3}$$

where k_i is a nodal value. For $n = 2$ we can get an average across or along a face of the test volume and with $n = 4$ we can get a volume average over the test volume. Note that in one dimensional heat conduction the harmonic average gives the effective conductance at the interface cf. [15], and from a material mixtures point of view the arithmetic and harmonic averages correspond to the Voigt and Reuss bounds, respectively.

The FVM directly employs finite differences for the temperature gradients. For regular meshes as typically employed for topology optimization, this provides first order accuracy of the heat flux at element boundaries. Volume integrals, such as the right hand side of equation (2), are defined as the average value over the element [14]. This corresponds to a linear interpolation over the element.

For a state element in the interior, equation (2) is evaluated as

$$-(\mathbf{q}_e \cdot \mathbf{n}_e + \mathbf{q}_w \cdot \mathbf{n}_w)h_y - (\mathbf{q}_n \cdot \mathbf{n}_n + \mathbf{q}_s \cdot \mathbf{n}_s)h_x = -f h_x h_y \tag{4}$$

where h_x, h_y are the element width and height, respectively. $\mathbf{q}_{(\cdot)} \cdot \mathbf{n}_{(\cdot)}$ is the outward normal heat flux at the element faces $\{w, e, s, n\}$ (for west, east, south, north). The flux is evaluated using a first order finite difference approximation e.g. for the west side with respect to $T_{i,j}$

$$\mathbf{q}_w \cdot \mathbf{n}_w = \langle k \rangle_w \frac{T_{i,j} - T_{i-1,j}}{\delta x}(-1) \tag{5}$$

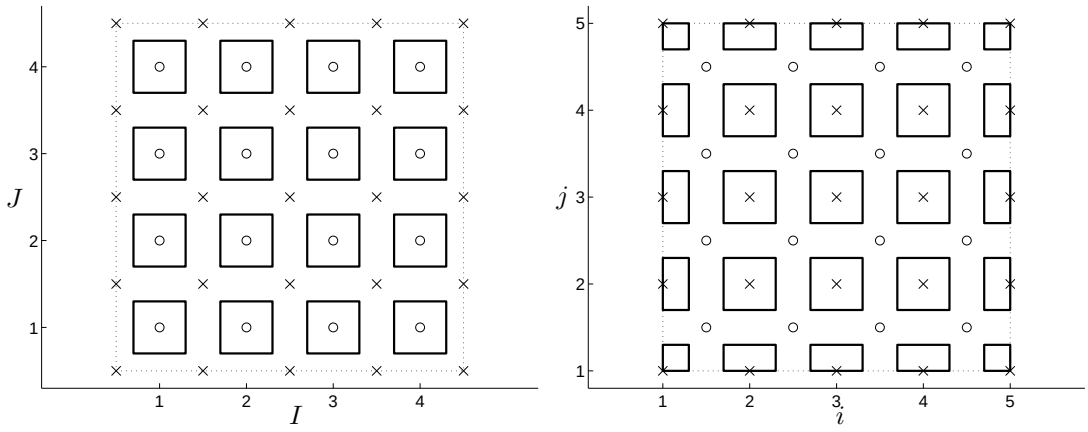

Figure 2: Sketch of finite volume discretization used. Design variables (conductivity) are cell centered '$\circ$' and forms the primal mesh with coordinates (I, J). State variables (temperature) are '$\times$' and forms the dual mesh with coordinates (i, j). For clarity, the volumes are shown somewhat shrinked – in the implementation they cover the domain completely. The physical boundary is represented by '$\cdots$'.

with δx being the x-distance between two temperature nodes. In the present case $\delta x = h_x$, cf., Fig. 2, except for boundary elements.

For the element with the state node $T_{i,j}$ we denote by $\tilde{\mathbf{u}}$ the vector that contains $T_{i,j}$ and the neighbors associated with a first order finite difference approximation

$$\tilde{\mathbf{u}} = \begin{bmatrix} T_{i-1,j} & T_{i+1,j} & T_{i,j-1} & T_{i,j+1} & T_{i,j} \end{bmatrix}^{\mathcal{T}} \tag{6}$$

with $(\cdot)^{\mathcal{T}}$ denoting the transpose operator. Then equation (4) for this node becomes

$$\begin{bmatrix} -\xi_w & -\xi_e & -\xi_s & -\xi_n & \sum \xi \end{bmatrix} \tilde{\mathbf{u}}_i = -f h_x h_y \tag{7}$$

where $\xi_{(\cdot)}$ is evaluated at the element faces

$$\xi_w = \frac{\langle k \rangle_w \, h_y}{\delta_x}, \;\; \xi_e = \frac{\langle k \rangle_e \, h_y}{\delta_x}, \;\; \xi_s = \frac{\langle k \rangle_s \, h_x}{\delta_y}, \;\; \xi_n = \frac{\langle k \rangle_n \, h_x}{\delta_y} \tag{8}$$

and $\sum \xi$ is the sum of the face contributions in equation (8).

Neumann boundary conditions fit directly into the FVM framework. For Dirichlet boundary conditions we here apply a penalty method, as suggested in [14] and [15].

Using a standard assembly procedure of the contributions (7) a matrix problem is obtained

$$\mathbf{K}\mathbf{u} = \mathbf{f} \tag{9}$$

where the matrix $\mathbf{K}$ is symmetric, $\mathbf{u}$ is the temperature vector and $\mathbf{f}$ the thermal load vector. The two vectors both contain nodal values defined at the center of the state elements.

One drawback of the FVM is the way boundary conditions at $\partial\Omega$ are treated; this complicates implementation. Also, the use of one–sided finite difference operators for elements at the boundary, means that special attention is needed in the solution of the state problem, and for optimization, in the evaluation of the cost functions and in the associated sensitivity analysis. Here we only illustrate the implementation for the interior elements and ignore the tedious treatment of the boundary elements.

5. Topology optimization

We consider here a generic topology optimization problem using the SIMP method [9]

$$\begin{aligned} \min_{\mathbf{a}\in\mathbb{R}^m} \quad & c(\mathbf{a}) \\ \text{s.t.} \quad & \sum_{i=1}^{m} A_i a_i \leq V^*,\ 0 < a_{min} \leq a_i \leq a_{max} \end{aligned} \tag{10}$$

where $\mathbf{a}$ are design variables, A_i element areas and $c(\mathbf{a})$ the cost function. The problem has a volume constraint in addition to the box constraints on the design variables, and the equilibrium equation $\mathbf{K}(\mathbf{a})\mathbf{u} = \mathbf{f}$ is assumed as the basis for evaluating $c(\mathbf{a})$. The conductivity $k = k(\mathbf{x})$ entering the matrix $\mathbf{K}$ is controlled by the design variables following a slightly modified SIMP-rule

$$\breve{\mathbf{k}} = \mathbf{s}(\mathbf{a}), \quad s_i(\mathbf{a}) = 10^{-3} + (1 - 10^{-3})a_i^p \tag{11}$$

where $\breve{\mathbf{k}}$ is a vector with nodal conductivity values and p is a penalty factor. The computational procedure used to solve (10) is in this work based on the use of the MMA algorithm [16], [17]. A continuation approach is adopted such that p is gradually increased to the final value $p = 3$ to obtain 0–1 designs (for details, see [9]).

5.1. Cost function

We consider here a cost function which is equivalent to compliance in structural problems. Physically, the optimization problem then corresponds to finding the conductivity distribution that produces the least heat, i.e., it is an optimal heat conducting device. For the continuum setting we have two equal expressions for the cost function:

$$c_I = -\int_\Omega fT \tag{12a}$$

$$c_{II} = \int_\Omega \nabla T \cdot \mathbf{q} = \int_\Omega \nabla T \cdot (k\mathbf{I}\nabla T) \tag{12b}$$

where $\mathbf{q}$ is the heat flux vector. For a FEM discretization we also have that $c_I = c_{II}$, in agreement with the principle of virtual work. However, this is not the case for the finite volume analysis. For a FVM implementation the use of c_I may be the natural choice (it does not involve derivatives). However, we here also consider c_{II} as one may in other optimization problems encounter situations where gradient expressions occur and it is thus relevant to understand how c_{II} can be handled in a FVM setting.

When using the FVM there is not a unique way to evaluate integrals such as (12b) as the variables are only available at specific points. Thus different FVM interpretations of c_{II} are available.

If we choose to treat the integrand similarly to the source term of the state equation one would apply straight averages. This gives a quadratic form in T:

$$c_{II}^q = \sum_{ne} \langle k \rangle_V (\nabla T \cdot \nabla T) A \tag{13}$$

where $\langle k \rangle_V$ is a volume average; choosing the arithmetic average corresponds to a linear interpolation of k over the element.

Alternatively, one can first rewrite c_{II} by applying the Green–Gauss theorem for (12b) and then use the strong form (1a):

$$\begin{aligned} c_{II} &= \sum_{ne} \int_{\Omega_e} \nabla T \cdot \mathbf{q} \\ &= \sum_{ne} \left\{ \int_{\partial\Omega_e} (T\mathbf{q}) \cdot \mathbf{n} - \int_{\Omega_e} fT \right\} \end{aligned} \tag{14}$$

where we now work with the normal heat flux across interfaces. This then can lead to the interpretation:

$$c_{II}^F = \sum_{ne} \{ \sum_{ef} \{ (\langle T \rangle^a \mathbf{q}) \cdot \mathbf{n} l \} - fTA \} \tag{15}$$

in which one applies an arithmetic average for the temperature $\langle T \rangle^a$ across a face. For the FVM the boundary contribution is zero because the flux is balanced and the average value $\langle T \rangle^a$ is the same across internal element boundaries, and thus $c_I = c_{II}^F$. The average temperature is used because a continuous temperature field is expected from a physical point of view.

As the form c_{II}^q is a quadratic form, this format is to be prefered, unless c_I is applied. To streamline the notation we define the finite difference operators using matrices

$$c_{II}^q = \sum_{ne} \tilde{\mathbf{u}}^{\mathcal{T}} \tilde{\boldsymbol{\mathcal{K}}} \tilde{\mathbf{u}} A \tag{16}$$

where $\tilde{\mathbf{u}}$ is given by equation (6), A is the element area and ne denotes the number of state elements. $\tilde{\boldsymbol{\mathcal{K}}}$ is symmetric and defined by

$$\tilde{\boldsymbol{\mathcal{K}}} = \langle k \rangle_V \mathbf{B}^{\mathcal{T}} \mathbf{B}, \quad \mathbf{B} = \begin{bmatrix} \frac{-1}{2h_x} & \frac{1}{2h_x} & 0 & 0 & 0 \\ 0 & 0 & \frac{-1}{2h_y} & \frac{1}{2h_y} & 0 \end{bmatrix} \tag{17}$$

where h_x and h_y are the element width and height, respectively.

5.1. Sensitivity analysis

We use the adjoint method to derive the sensitivity $\frac{\mathrm{d}c}{\mathrm{d}a_i}$ needed by a gradient driven optimization algorithm (cf., e.g., [19]). The sensitivity analysis can be done analytically when using c_I, but for c_{II} the solution of an adjoint problem is required.

We first write a Lagrangian in the form

$$\mathcal{L} = \mathbf{u}^{\mathcal{T}} \tilde{\mathbf{K}} \mathbf{u} + \boldsymbol{\lambda}^{\mathcal{T}} \left(\mathbf{K}\mathbf{u} - \mathbf{f} \right) \tag{18}$$

where $\tilde{\mathbf{K}}$ is an assembled version of (17) and $\mathbf{f}$ is independent of the design. This – by standard derivation – gives the sensitivity as

$$\frac{\mathrm{d}c}{\mathrm{d}a_i} = \frac{\mathrm{d}s_j}{\mathrm{d}a_i} \left(\mathbf{u}^{\mathcal{T}} \frac{\partial \tilde{\mathbf{K}}}{\partial s_j} + \boldsymbol{\lambda}^{\mathcal{T}} \frac{\partial \mathbf{K}}{\partial s_j} \right) \mathbf{u} \tag{19}$$

where $\boldsymbol{\lambda}$ is the solution to the adjoint problem

$$\mathbf{K}^{\mathcal{T}} \boldsymbol{\lambda} = - \left(\tilde{\mathbf{K}} + \tilde{\mathbf{K}}^{\mathcal{T}} \right) \mathbf{u} \tag{20}$$

Since $\mathbf{K}$ is symmetric the adjoint problem is efficiently solved using back substitution. Note, that the cost function matrix $\tilde{\mathbf{K}}$ is not necessarily symmetric for some interpretations of c_{II}, but for c_{II}^q it is symmetric. Also note, that the result is somewhat different from what is typpically seen for FEM, due to the fact that in FVM the matrices $\mathbf{K}$ and $\tilde{\mathbf{K}}$ do not coincide.

The implementation of the above follows standard adjoint sensitivity analysis procedures with a slight deviation when calculating $\frac{\partial \mathbf{K}}{\partial s_i}$. As depicted in figure 3 each design variable enters in the system matrix $\mathbf{K}$ in four rows through the averages cf. equation (7)-(8). Thus we find

$$\frac{\partial \mathbf{K}}{\partial s_i}\mathbf{u} = \begin{bmatrix} {}^1\xi'_e + {}^1\xi'_n & -{}^1\xi'_e & 0 & -{}^1\xi'_n \\ -{}^2\xi'_w & {}^2\xi'_w + {}^2\xi'_n & -{}^2\xi'_n & 0 \\ 0 & -{}^3\xi'_s & {}^3\xi'_s + {}^3\xi'_w & -{}^3\xi'_w \\ -{}^4\xi'_s & 0 & -{}^4\xi'_e & {}^4\xi'_s + {}^4\xi'_e \end{bmatrix} \begin{bmatrix} {}^1u \\ {}^2u \\ {}^3u \\ {}^4u \end{bmatrix} \tag{21}$$

using the notation shown in figure 3. For the test examples presented below the sensitivities were checked using a finite difference approximation.

6. Test problems

Two types of test problems have been investigated. They differ by the types of boundary conditions that are considered for the reference domain Ω, which in both cases is the unit square. One problem has the total length of the west and north boundaries of Dirichlet type, cf., figure 4(d), so that for a homogeneous lay-out, high regularity of the state is to be expected and thus FEM and FVM should be completely similar. The other problem has only

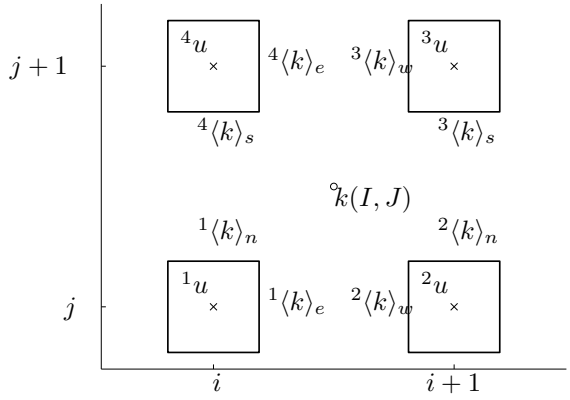

Figure 3: Link between node $k(I,J)$ and the face conductivities $\langle k\rangle_{(\cdot)}$ at surrounding state elements. The state elements are numbered counter–clockwise ${}^1u,\ldots,{}^4u$ to clarify the implementation.

a small part of the west boundary with a Dirichlet boundary condition, cf., figure 6(d), so here low regularity is expected and the boundary condition is tricky to implement. Here one sees that FVM and FEM behaves somewhat differently even for the homogeneous case. However, the designs that are obtained are similar in nature.

The volumetric forcing is $f = 10^{-2}$ in both problems. The filter proposed by Sigmund (see [20], [9]) is used in some examples; this can control the formation of checkerboards and control geometry. Here, the filter radius is chosen so that only checkerboards are removed and it does not impose geometry constraints on the design beyond the mesh scale (the filter is thus here mesh-dependent).

6.1 Case 1

Figure 4 shows the final designs for the minimization of the cost function c_I using a finite element approach and using the FVM with the arithmetic average (FVM_a) as well as the harmonic average (FVM_h). Using the FVM_a without filtering led to the same time of checkerboards taht are well known from topology optimization using FEM. The checkerboards can be removed by the filtering mentioned above or by using the harmonic average in the FVM formulation. The designs obtained are qualitatively similar to results obtained by [12] for pressurized membranes, which are also governed by the Poisson equation.

For the FVM_a, the value of c_I is smaller than c_I evalutated using the FEM, cf., Fig. 4(e) which shows that a (local) discrete optimum has been found compared with the FEM. Using the FVM_h this is not the case, cf., Fig. 4(f) due to the the material averaging scheme used.

Using continuation and a final penalization value $p = 5$ reduces the amount of intermediate densities, which appear using the harmonic average. In addition, computations show that constructing an average of the material properties being a linear combination of the arithmetic and harmonic average gives control of the amount of intermediate densities/checkerboards without filtering of the sensitivities.

Designs obtained using the cost function c_{II}^q are seen in figure 5. They are qualitatively similar to the designs obtained using the cost function c_I, cf., figure 4.

6.2 Case 2

This problem has a solution that is less regular than the previous test problem since the change from the Dirichlet to the Neumann boundary condition does not happen at a corner, cf., Fig. 6(d). The FEM framework is able to handle such an abrupt change in the boundary conditions, whereas the FVM which is based on the strong form has problems – this is evident from a convergence study of a uniform design (this discussion is beyond the scope of this paper). However, figure 6(a)-6(c) show that for the present topology optimization problem this does not render qualitative differences. Similar FEM results are presented in [12] and [9].

Figure 6(e) illustrates a possible future application of topology optimization in urban planing tasks such as the metro layout shown in figure 6(f). One may also think that escape route layouts on music festivals and in large

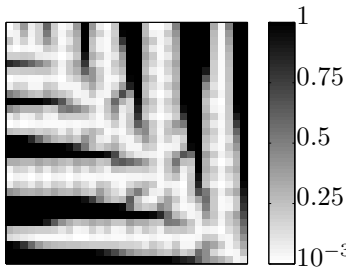

(a) FEM^f, with filter. 32×32 design variables, $c_I = 5.10 \times 10^{-5}$.

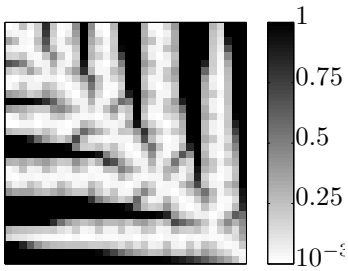

(b) FVM_a^f (arithmetic), with filter. 32×32 design variables, $c_I = 4.97 \times 10^{-5}$.

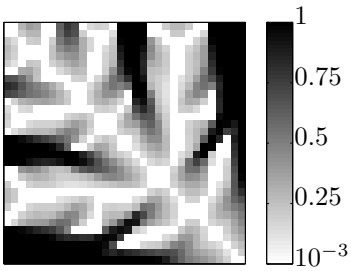

(c) FVM_h (harmonic), no filter. 32×32 design variables, $c_I = 7.27 \times 10^{-5}$.

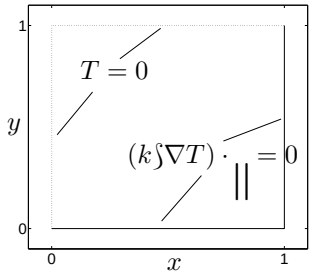

(d) Boundary conditions. $T = 0$ on west and north side '$\cdots$' and $(k\boldsymbol{I}\nabla T) \cdot \boldsymbol{n} = 0$ on east and south side '–'.

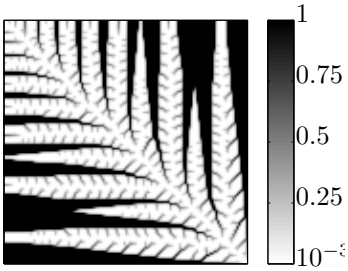

(e) FVM_a^f (arithmetic), with filter. 128×128 design variables, $c_I = 3.82 \times 10^{-5} < c_I^{FEM} = 3.86 \times 10^{-5}$.

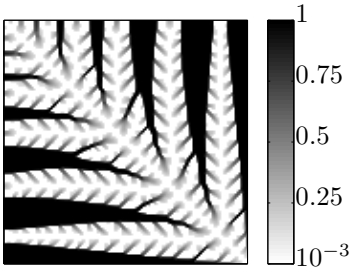

(f) FVM_h (harmonic), no filter. 128×128 design variables, $c_I = 4.58 \times 10^{-5} > c_I^{FVM_a} = 4.02 \times 10^{-5} < c_I^{FEM} = 4.04 \times 10^{-5}$.

Figure 4: Design examples with the cost function c_I with $V^* = 0.4$. Boundary conditions are seen in figure 4(d). For the designs in figure 4(c) and 4(f) no filter is used. The sensitivities have been filtered using the Sigmund filter (see [20]) for the designs in figures 4(a), 4(b) and 4(e).

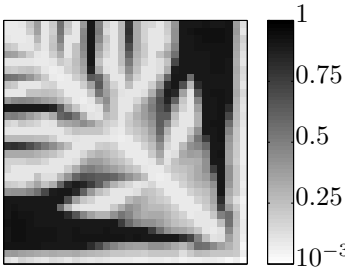

(a) FVM_a^f (arithmetic), with filter. $c_{II}^q = 7.12 \times 10^{-5}$.

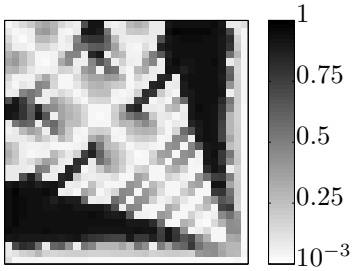

(b) FVM_h (harmonic), no filter. $c_{II}^q = 6.25 \times 10^{-5}$.

Figure 5: Designs obtained for the cost function c_{II}^q. Design examples with 32×32 design variables, $V^* = 0.4$ and boundary conditions seen in figure 4(d).

sports arenas would benefit from using topology optimization. The latter cases enjoy the property of being planar problems with constant population density similar to the volumetric heating used in the present note.

7. Discussion

The present work demonstrates that topology optimization is possible in a finite volume setting and that it requires minor deviations in the sensitivity analysis compared to a conventional finite element implementation.

A number of topology optimization problems have been solved on a staggered mesh using the arithmetic and harmonic average for interpolation between nodal values of material data. This is consistent with the finite volume method and the averages correspond to the well known Voigt and Reuss bounds. The use of the arithmetic average gives rise to the formation of checkerboards during the optimization process, but they can be avoided by the implementation of a sensitivity filtering. However, when using the harmonic average, checkerboards do not form and by combining the arithmetic and harmonic averages one obtains control of the amount of checkerboards in the design without filtering of the sensitivities.

Boundary conditions are handled differently in the finite volume method compared to the finite element method, in particular in the case of lack of boundary regularity. One such problem is considered and it appears that the difference does not play a qualitative role for the design.

8. Acknowledgements

The first author thanks Per Grove Thomsen, Martin Berggren, Christian Lotz Felter, Bjarne Skovmose Kallesøe, and Dalibor Cavar for helpful discussions related to this work. This work received financial support from Denmark's Technical Research Council (the "Phonon project").

9. References

[1] Borrvall T, Petersson J (2003) Topology optimization of fluids in Stokes flow. *Int. J. Num. Meth. Fluids* **41**, 77–107.

[2] Sigmund O, Gersborg-Hansen A, Haber RB (2003) Topology optimization for multiphysics problems: A future femlab application? In: Gregersen, L. (ed.) *Nordic Matlab Conference (held in Copenhagen)*,pp. 237–242. Søborg, Denmark: Comsol

[3] Gersborg-Hansen A, Sigmund O, Haber RB (2005) Topology optimization of channel flow problems. *Struct. Multidisc. Optim.*, to appear.

[4] Olesen LO, Okkels F, Bruus H (2005) A high–level programming–language implementation of topology optimization applied to steady-state Navier–Stokes flow. *Submitted*. Available at: http://www.mic.dtu.dk/research/MIFTS/publications/pub2004/topopt.pdf

[5] Jenny P, Lee SH, Tchelepi HA (2004) Adaptive multiscale finite-volume method for multiphase flow and transport in porous media. *Multiscale Model. Simul.* **3**(1), 50-64.

[6] Barth T, Ohlberger M (2004) Finite volume methods: Foundation and analysis. Volume 1, chapter 15 in *Encyclopedia of computational Mechanics*, editors: Stein, E.; Borst, R., Hughes, T. J. R. West sussex, England: John Wiley & Sons

[7] Chalot FL (2004) Industrial aerodynamics. Volume 3, chapter 12 in *Encyclopedia of computational Mechanics*, editors: Stein, E.; Borst, R., Hughes, T. J. R. West sussex, England: John Wiley & Sons

[8] Vos JB et al. (2002) Navier-Stokes solvers in European aircraft design. *Progress in Aerospace Sciences* **38**, 601-697.

[9] Bendsøe MP, Sigmund O (2004) *Topology Optimization - Theory, Methods, and Applications*. Berlin Heidelberg: Springer Verlag

[10] Sigmund O (2001) Design of multiphysics actuators using topology optimization - Part I: One-material structures. *Comput. Mehtods Appl. Mech. Eng.* **190**(49-50), 6577–6604.

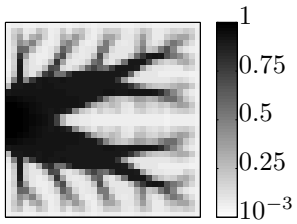

(a) FEM, with filter, $\gamma = 1/32$. 32×32 design variables and $V^* = 0.4$. $c_I = 2.49 \times 10^{-4}$.

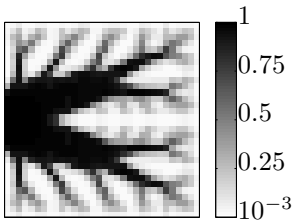

(b) FVM_a^f (arithmetic), with filter, $\gamma = 1/32$. 32×32 design variables and $V^* = 0.4$. $c_I = 2.13 \times 10^{-4}$.

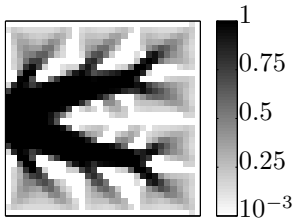

(c) FVM_h (harmonic), no filter, $\gamma = 1/32$. 32×32 design variables and $V^* = 0.4$. $c_I = 2.37 \times 10^{-4}$.

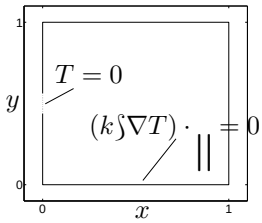

(d) Boundary conditions. $T = 0$ on a fraction γ of the west side '$\cdots$' and $(k\boldsymbol{I}\nabla T) \cdot \boldsymbol{n} = 0$ on Γ_N '–'.

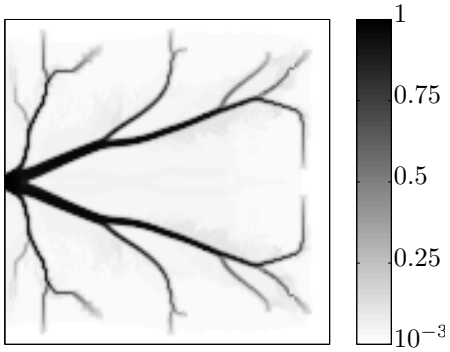

(e) FVM_a^f (arithmetic), with filter, $\gamma = 1/128$. 128×128 design variables. $V = 0.1$.

(f) Plan of possible extensions (colored lines) of the Copenhagen Metro. From the [21].

Figure 6: Designs obtained for the cost function c_I measuring the non–smooth temperature field caused by the boundary conditions seen in figure 6(d). The difference in the way the FEM and the FVM handles the non–smooth boundary conditions does not yield a qualitative difference in the design. Figure 6(e) illustrates a possible future application in urban planing tasks such as the metro layout shown in figure 6(f). One may also think that escape route layouts on music festivals and in large sports arenas may benefit from using topology optimization.

[11] Sigmund O (2001) Design of multiphysics actuators using topology optimization - Part II: Two-material structures. *Comput. Mehtods Appl. Mech. Eng.* **190**(49-50), 6605–6627.

[12] Donoso A, Sigmund O (2004) Topology optimization of multiple physics probelms modelled by Poisson's equation. *Latin Amr. J. Solid Struc.*, **1**, 169-184.

[13] Diaz AR, Benard A (2003) Topology optimization of heat-resistant structures. *Proceedings of the ASME Design Engineering Technical Conference*, **2A**, 633-639.

[14] Versteeg HK, Malalasekera W (1995) An introduction to Computational Fluid Dynamics: the Finite Volume Method. London: Longman Scientific & Technical

[15] Patankar SV (1980) Numerical heat transfer and fluid flow. Hemisphere Publishing Corporation

[16] Svanberg K (1987) The method of moving asymptotes – a new method for structural optimization. *Int. J. Numer. Meth. Eng.* **24**, 359-373.

[17] Svanberg K (2002) A class of globally convergent optimization methods based on conservative convex separable approximations. *SIAM Journal on Optimization*, **12**(2), 555-573.

[19] Choi KK, Kim N-H (2005) *Structural Sensitivity Analysis and Optimization 1 & 2*. Berlin Heidelberg: Springer Verlag

[20] Sigmund O (2001) A 99 line topology optimization code written in MATLAB. *Struct. Multidisc. Optim* **21**, 120–127. MATLAB code available online at: www.topopt.dtu.dk

[21] The Danish Ministry of Transport (2004) Udredning om Cityringen. ISBN: 87-91013-51-8.